Physics – Uspekhi **62** (9) 931 – 940 (2019)

INSTRUMENTS AND METHODS OF INVESTIGATION PACS numbers: **28.60.+s**, **29.25.–t**, 87.57.U–

Molybdenum-99 production via lead and bismuth moderators and milli-structure-^{98}Mo samples by the indirect production technique using the Monte Carlo method

A Khorshidi

DOI: https://doi.org/10.3367/UFNe.2018.09.038441

Contents

Abstract. We describe the design of a neutron activator that contains a beryllium target, a lead/bismuth moderator, graphite/PbF_2 reflectors, and a boron absorber. Production of the ^{99}Mo isotope using millimeter-sized ^{98}Mo samples located in various regions of the activator was simulated using the MCNPX code. If the ^{98}Mo samples are placed in the reflector region, the yield increases due to a larger flux of epithermal neutrons.

Keywords: neutron activator, neutron moderator material, adiabatic resonance crossing, radioisotope production, molybdenum transmutation, nuclear medicine, Monte Carlo method

1. Introduction

^{99m}Tc is the most commonly used medical radionuclide for imaging in nuclear medicine. ^{99}Mo with a half-life of 69.5 hours is the radioisotope used as a generator for the production of ^{99m}Tc, accounting for approximately 80% of the total number of medical procedures using radioisotopes [1–4]. It emits 140.5 keV γ-rays, and a lesion location within the body can be accurately detected by single photon emission computed tomography (SPECT) imaging using a collimated γ-ray camera with adequate efficiency and resolution [5–10]. In addition, it can be used to monitor heart and liver functions and to map blood flow in the brain and guide operations [11–14].

Alternative radiopharmaceutical nuclides, like ^{99}Mo, have drawn considerable attention. Today, most of the ^{99}Mo is produced by the fission reaction of highly enriched (HEU) or low-enriched (LEU) Uranium-235 in many reactors around the world [15, 16]. Neutron capturing in the resonance peak range, a method proposed by Rubbia in 1997 [17] and called the ARC technique, can activate some elements and transmutation of nuclear wastes [18–21]. In 1995, Rubbia et al. [22] designed an accelerator-driven method to eliminate waste material from nuclear reactors and economically detect long-lived fission fragments using the ARC technique. The subcritical very fast neutron core driven by a proton accelerator has been used as an energy amplifier. The potential of transmutation in transuranium elements was verified in [23–27]. Moreover, in [28–30] driven-technique-based accelerators were presented that take up neutrons and then indirectly produce medical radioisotopes.

In this study, a neutron activator based on the cyclotron located in Karaj, Iran (from IBA, Belgium, Cyclon30) is simulated in the indirect production method based on the ARC technique to evaluate the ^{98}Mo production yield. Simulations are done in order to competently operate ion-beam-created fast neutrons to produce radionuclides in the activator regions, including the moderator, reflector, and absorber parts. Monte Carlo *N*-article code version X 2.6 (MCNPX) [31] simulations are planned to investigate a new neutron activator scheme from a 30 MeV incident proton in a 300 μA current, bismuth and lead moderators, graphite and lead(II) fluoride reflectors, and a boron absorber to estimate the accumulated neutron flux. The goal of this study is to optimize the proposed scheme based on low-current and low-energy protons via target design, the type of moderator and reflector materials, and the enriched milli-structure-^{99}Mo samples thicknesses at various positions to evaluate activity

A Khorshidi Paramedical School, Gerash University of Medical Sciences, Gerash, Iran
E-mail: abkhorshidi@yahoo.com

Received 26 April 2018, revised 3 September 2018
Uspekhi Fizicheskikh Nauk **189** (9) 997 – 1007 (2019)
DOI: https://doi.org/10.3367/UFNr.2018.09.038441
Edited by A M Semikhatov

and ^{99}Mo production yield through capturing moderated neutrons.

2. Methods and materials

2.1 Target design for a neutron generator system

Target preparation for radioisotope production has to take balance into consideration, along with mechanical, thermal, and neutron characteristics. Producing an adequate number of neutrons by an incident proton beam is one of the most important properties in target design. Undoubtedly, heat spreading over the target area when the charged particle beam hits it must be as large as possible to avoid melting the target. In this study, however, the heat spreading should be small enough to reduce the loss of neutrons produced near the target edges. When the protons are stopped in the target, heat is generated. Thus, a heat reduction system should be in place around the target for the purpose of cooling and maintaining mechanical stability. The cooling system around the target affects the neutron field. Therefore, it should be integrated into the moderator configuration to prevent it from changing the proper neutron energy spectrum by diminishing the neutron flux. A 30 MeV incident proton beam on the target area with a 300 μA current produces 9 kW of heat power in the target volume.

A cylindrical shape with a length of 1 cm and a radius of 0.83 cm was designed and the axis of the proton beam was perpendicular to the base of the shaped target. Beryllium (Be) was chosen as the target material due to its high melting point (1287 °C) and high mechanical durability. The density of the Be target is 1.85 g cm^{-3}, and the projected range in the Be target is 0.580 cm for an energy of 30 MeV of the incident proton. A water cooling system was also considered around the target. The thermo-hydraulic outline of the target water cooling system was designed using Ansys software and computational fluid dynamics (CFD) methods [32]. The software was used to estimate the target temperature, the cooling water velocity, and the temperature distribution around the target with specified boundary conditions.

The number of neutrons generated per area and per second from proton interactions inside a layer of a thickness dx in the target is

$$\mathrm{d}S = Nj\sigma\,\mathrm{d}x\,, \tag{1}$$

where σ [cm^2] is the microscopic cross section, N (nucleus per cm^3) is the target nuclide density, and j is the beam intensity in protons cm^{-2} s^{-1}. Equation (1) is only valid for small depths x because it ignores the reduction in intensity as a function of depth. In integrating Eqn (1) to find the total yield, we note that the cross sections of the neutron-generating nuclear reactions change rapidly with the energy of the initiating proton particles, which are slowed down rapidly by Coulomb interaction with the electrons in the target. Therefore, the ratio S/j can be calculated as

$$\frac{S}{j} = N\int_0^{E_0}\frac{\sigma(E)\,\mathrm{d}E}{\mathrm{d}E/\mathrm{d}x} = N\sigma R = \frac{R}{\lambda}\,, \tag{2}$$

where R is the reaction rate, λ is the mean free path of the proton downstream, and $\mathrm{d}E/\mathrm{d}x$ is the stopping power, expressed in MeV cm^{-1}. Equation (2) assumes that σ is constant, whereas it is a function of the proton energy. In addition to that, the thick target yield (TTY) of neutrons in a differential analysis is determined as

$$\frac{\mathrm{d}^2Y(E_0)}{\mathrm{d}E\,\mathrm{d}\Omega} = N\int_0^X \frac{\mathrm{d}^2\sigma\left(E_0 - \int_0^x(\mathrm{d}E/\mathrm{d}x)\,\mathrm{d}x\right)}{\mathrm{d}E\,\mathrm{d}\Omega} \times \exp\left[-N\sigma_{\mathrm{nonel}}\left(E_0 - \int_0^x\left(\frac{\mathrm{d}E}{\mathrm{d}x}\right)\mathrm{d}x\right)x\right]\mathrm{d}x \quad \mathrm{n/MeV/Sr/projectile}\,, \tag{3}$$

where the incident particle energy is E_0 [MeV], the target thickness is X [cm], and the inelastic cross section is σ_{inel} [cm^2]. Here, the ^{9}Be(p.xn) reaction was simulated using the Bertini physics model. This model applies pre-equilibrium, intra-nuclear cascade procedures and elastic scattering for protons and neutrons. The neutrons produced by proton interactions are sent out around the circumscribed target and the transport behavior of induced neutrons has a connection with diffusion materials enclosed in the target. All the pertinent cross sections were derived in the simulations from ENDF/B-VII.1, 2011 libraries.

2.2 Design of moderator and reflector regions

The accelerator-driven procedure in radioisotope production via transmutation was modeled in three steps: neutron production, moderation, and capture. The Monte Carlo method was used to simulate the neutron activator via a 30 MeV proton source to check neutron transport in the moderator and reflector structures. The materials used in this study were chosen so as to reach an adequate neutron flux [33].

Investigations via low-current protons incident on the beryllium target were carried out to drive the neutron activator. The moderation of induced neutrons is a process of slowing down fast neutrons during interactions with the nuclei of the moderator material. Having collided with the nucleus, neutrons lose momentum and decelerate until the instant when they are in thermal equilibrium with the medium they are moving through [16, 34, 35]. Bismuth and lead are elements of high atomic weights, characterized by high inelastic and elastic cross sections for high-energy neutrons (above 1 MeV) and low capture cross sections. Elastic cross sections of heavy nuclides like bismuth and lead are considerably different from those of light nuclides like hydrogen, deuterium, graphite, and oxygen. For these light nuclides, neutron deceleration from 0.1 MeV to 0.5 eV respectively requires 12, 17, 77, and 102 elastic collisions on average. The same neutron deceleration requires about 1269 elastic collisions in natural lead [36]. The high atomic mass of bismuth and lead makes it rational to use them as a moderator material instead of other light materials.

Because the cross section of neutron capture at the epithermal range and the captured resonance integral for bismuth and lead are much greater than the corresponding quantities for light nuclides, it can be predicted that there is a higher probability of moderated neutrons to be captured in bismuth or lead during moderation. On the other hand, the numerous moderated neutrons would continuously and gradually decelerate toward the epithermal range. Therefore, it can be assumed that a greater epithermal flux must be achieved even with the multiple scattering of neutrons using the two proposed moderators.

The reflecting process along with moderation can increase the chances of neutron capture. Therefore, selecting an effective material for reflecting neutrons would be significant in transmutation. Graphite is typically used in most nuclear reactors to reflect the neutrons toward uranium to bring

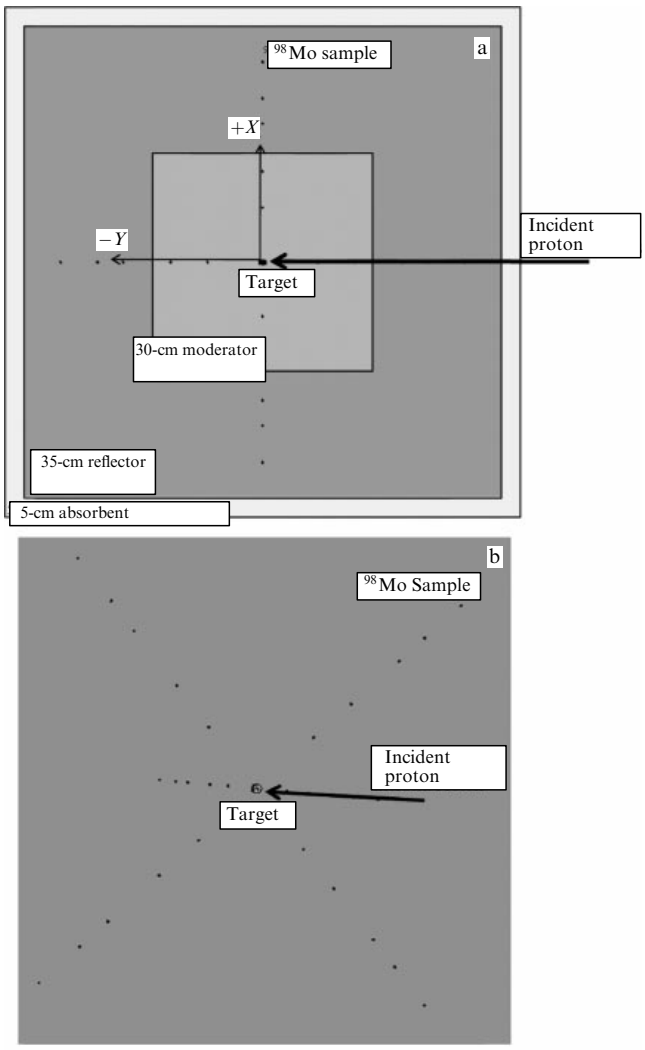

Figure 1. (a) Cubic model of a neutron activator containing a neutron generator and moderator, surrounded by a reflector and absorber. (b) Positions of ^{98}Mo samples at various distances from the target.

about further fission [37, 38]. A suitable reflector is a material that is likely to scatter neutrons backwards in a wide range of energies. Therefore, to assess the reflecting material, PbF_2 is presented in this study as a neutron reflector for radioisotope transmutation via the indirect method.

In this situation, molybdenum transmutation via the ARC technique and indirect production method in accelerator-driven systems was simulated. The configuration of the neutron activator is shown in Fig. 1a with different regions as regards the interaction space of generated neutrons. The moderator region, which is 30 cm thick, is surrounded by a 35 cm thick cubic graphite reflector. The third region is made of 5 cm thick boron to absorb the wasted neutrons. To simulate the neutron activator in order to estimate the production yield via radiative capture reaction, $^{98}\mathrm{Mo}(\mathrm{n},\gamma)\,^{99}\mathrm{Mo}$, bismuth, and natural lead moderators, besides graphite and PbF_2 reflectors, were proposed to produce thermal and epithermal neutron flux spectra.

2.3 Distribution of milli-structure-^{98}Mo in a neutron activator

Spheres with the radii of 1 mm and 2 mm were simulated and distributed at various distances from the target (Fig. 1b): 15 cm and 25 cm in the moderator area, and 38 cm, 45 cm, and 55 cm in the reflector area for x, y, and z directions, respectively.

The abundance of ^{98}Mo is about 25%, and the $^{98}\mathrm{Mo}(\mathrm{n}_{\mathrm{epithermal}},\gamma)\,^{99}\mathrm{Mo}$ reaction just includes moderated neutrons. The maximum cross section of radiative capture in ^{98}Mo is of the order of 100 barn. Therefore, the generated neutrons should be decelerated from the original energy to a qualified energy throughout collisions with the heavy nuclei of the moderator. To assess the ^{99}Mo production yields inside the different regions of the activator, the obtained data were normalized to the enriched sample mass and to the proton current. Hence, the production yield (MBq g^{-1}) was defined as

$$\text{production yield} = \frac{A_0}{m_{\mathrm{s}}\left[1-\exp\left(-\ln\left(2\right)T_{\mathrm{run}}/T_{1/2}\right)\right]}\,, \quad (4)$$

where A_0 is the activity at saturation, T_{run} is the time of operation, m_{s} is the ^{98}Mo sample mass, and the half-life of the produced ^{99}Mo radioisotope was set as $T_{1/2}$ via ENDF/B-VII.1 libraries of cross sections. During the running by the MCNP code, incident protons on the beryllium target generate induced neutrons that spread out toward the moderator area in 4π space. The neutron activator was delineated in two moderators/reflectors, with the number of incidents being 10^7. The volume-track-length tally in the code was used as the scoring data, equal to the distances traveled by a particle in a determined volume. This tally was normalized to time and volume in terms of particle cm^{-3} s^{-1} in output data. Particle transport options were considered such as absorption, elastic/inelastic scattering angular distribution, and anisotropic reactions via point cross section modules.

2.4 Statistical procedure in the MCNP code

The MCNP code produces an output file that includes valuable information about the simulation. To diminish the estimated expense, a tally assessment with logical relative error is desired. Any input file should include enough incidents to achieve an acceptable output, taking computer time into consideration. Reduction in relative error of a tally at a fixed computing time results in an acceptable response and also reduces the relevant variance.

After running a text-input file via the code, the ith history gives an x_i-score in the tally's log. The range of the values of this record is between zero (when the particle never reaches the tally region) and a very large value (when the particle reaches the tally without any interaction). On the other hand, the probability of any incident gives a $p(x)\,\mathrm{d}x$ score in the range from x to $x+\mathrm{d}x$; here, $p(x)$ is the probability distribution function (PDF) such that the mean, or expectation value of x is defined as

$$\langle x\rangle \equiv \int_0^X xp\,(x)\,\mathrm{d}x\,. \quad (5)$$

The function $p(x)$ is initially undetermined; therefore, the code approximates the mean of $\bar{x}$, $\langle x\rangle$, from scores of N particles:

$$\bar{x} \equiv \frac{1}{N}\sum_{i=1}^{N} x_i\,. \quad (6)$$

Acquiring a finite value of $\langle x\rangle$ requires that $N\to\infty$ such that $\bar{x}\to\langle x\rangle$. The standard deviation of the histories is used to

show variation in the various x_i values:

$$S^2 \equiv \frac{1}{N-1}\sum_{i=1}^{N}(x_i-\bar{x})^2 \cong \overline{x^2}-\bar{x}^2\,, \tag{7}$$

where

$$\bar{x}^2 = \frac{1}{N}\sum_{i=1}^{N} x_i^2\,. \tag{8}$$

Therefore, the estimated variance of the mean $\bar{x}$ is

$$S_{\bar{x}}^2 \equiv \frac{1}{N}\,S^2\,. \tag{9}$$

If the simulation is repeated with N histories a large number of times, the deviations of the means $\bar{x}$ from each record would normally distribute around the right mean $\langle x\rangle$ and contain a variance $S_{\bar{x}}^2$. This invokes the central limit theorem via repetition of the simulation. The variance or uncertainty should be reduced in simulations as the minimum $S_{\bar{x}}$ is estimated for a fixed number of incident particles $S_{\bar{x}}^2$ [39]. To concentrate the $p(x)$ distribution around its mean $\langle x\rangle$ for any simulation, the variance reduction technique was used by producing fewer zero-sore records. This technique maintains the mean of the analog PDF as the variance of the mean $S_{\bar{x}}$; therefore, the estimation of the median value is more precise.

Another statistical quantity that can be calculated by the MCNP code is the relative error R,

$$R \equiv \frac{S_{\bar{x}}}{\bar{x}}\,. \tag{10}$$

The R parameter should be as small as possible and must be less than 0.1 for meaningful records. This parameter estimates the uncertainty in the tally mean with a 1-sigma fraction as $R \equiv S_{\bar{x}}/\bar{x}$, the proportion of the standard deviation of tally mean per mean.

Another important parameter generated by the code is the figure of merit (FOM), defined as [31]

$$\mathrm{FOM} = \frac{1}{R^2 T_{\mathrm{run}}}\,, \tag{11}$$

where T_{run} is the time of the run. The value of T_{run} depends on the computer used, and then similar simulations should be run on various machines to generate distinctive FOMs. In the variance reduction method, the largest value of FOM should be selected.

The precision of the tally mean was evaluated by the relative error R, and the accuracy of R can be estimated via the relative variance of R, termed the variance of a variance (VOV), defined as [31]

$$\mathrm{VOV} = \frac{S^2(S_{\bar{x}}^2)}{S_{\bar{x}}^4} = \frac{\sum_{i=1}^{N}(x_i-\bar{x})^4}{\left[\sum_{i=1}^{N}(x_i-\bar{x})^2\right]^2}\,\frac{1}{N}\,, \tag{12}$$

where $S^2(S_{\bar{x}}^2)$ is the variance of $S_{\bar{x}}^2$. The VOV parameter includes the 3rd and 4th moments of the $f(x)$ tally distribution, but the parameter R is based on only the first and second moments of $f(x)$. The VOV parameter is more sensitive to fluctuations in large sets than R is. A suitable sampling of infrequent but large histories is crucial if credible tally means are to be acquired. Equation (12) demonstrates that the VOV parameter ought to reduce as $1/N$. The MCNP code can examine this performance in the VOV parameter to reach an acceptable record of less than 0.1 for any type of calculation.

3. Results and discussion

3.1 Neutron yield and flux exploration for various moderators and reflectors

A neutron activator was recommended for low-energy and low-current protons through high-atomic-mass moderators

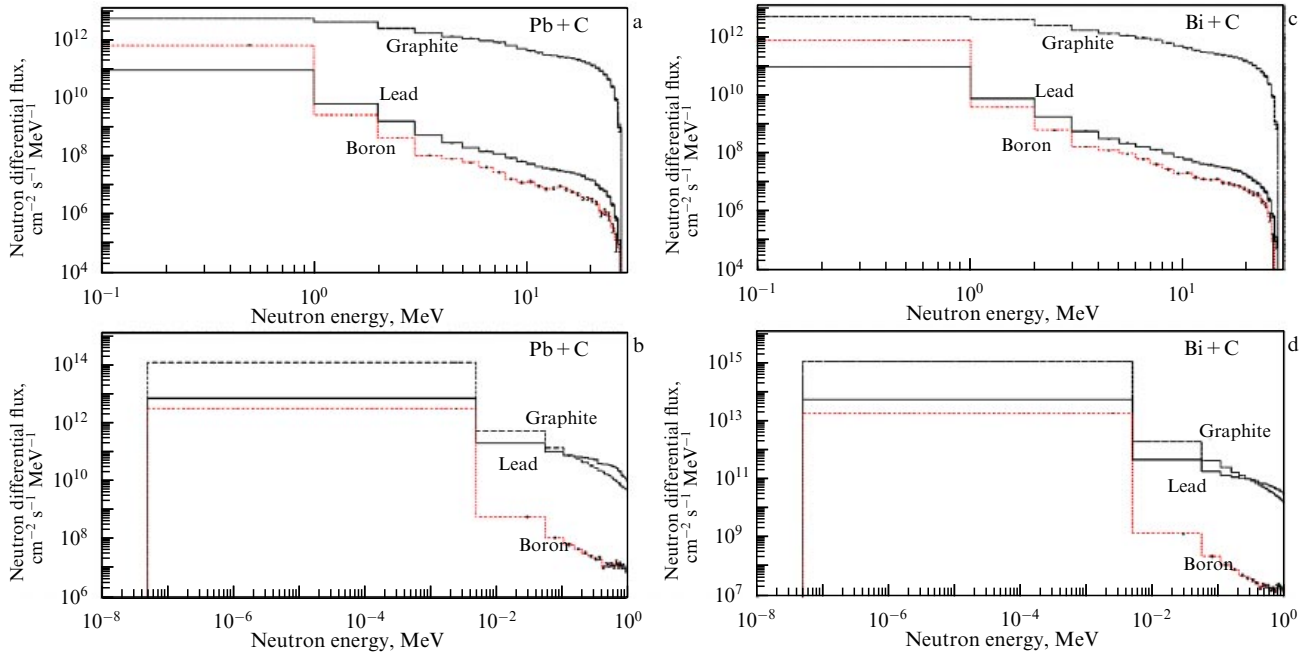

Figure 2. (a) Total flux of neutrons derived from a beryllium target inside lead, graphite, and boron regions using a graphite reflector. (b) Fast neutron flux inside lead, graphite, and boron regions using a graphite reflector. (c) Total flux of neutrons derived from a beryllium target inside bismuth, graphite, and boron regions using a graphite reflector. (d) Fast neutron flux inside bismuth, graphite, and boron regions using a graphite reflector.

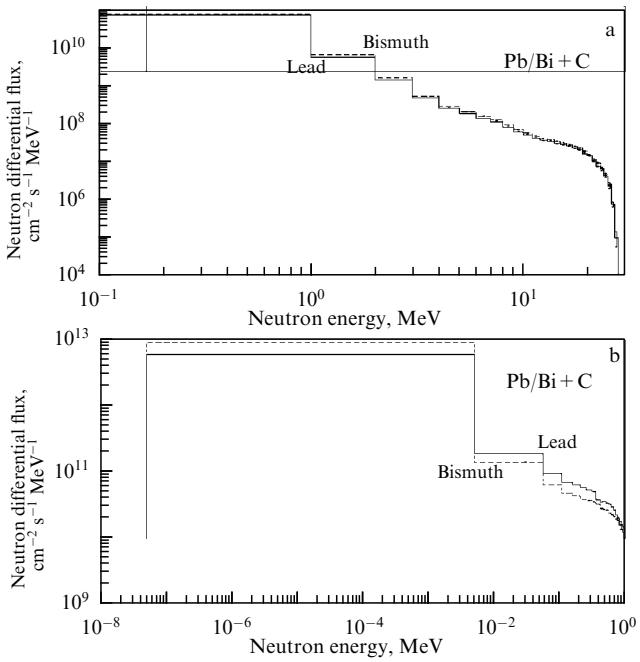

Figure 3. (a) Total flux of neutrons using graphite reflector for the comparison of lead and bismuth moderators. (b) Fast neutron flux using graphite reflector for the comparison of lead and bismuth moderators.

and two types of reflectors via a neutron generator system. Target disintegration from the interaction between the incident proton beam and the target nuclei depends on the energy range of the proton and on the physical features of the target. The total number of neutrons generated per second at 300 μA was 3.60×10^{13}n s^{-1} on the target, with the neutron-to-proton ratio estimated to be 0.0192 at 1 μA of the incident proton. The method in [17] gives the number of neutrons generated by proton interaction. Also, a parametric CFD analysis of the target configuration was used to determine the cooling conditions: the single-phase cooling flow, the limited flow velocities, and smooth temperature gradients in the target body. Using a 30 MeV, 300 μA proton beam, a water flow rate of 0.901 s^{-1}, and an inlet water temperature of 13 °C, the maximum calculated temperature in the Be target was 489.15 °C. The maximum temperature in the solid target does not reach the melting point of Be (1287 °C).

The neutrons induced from incident protons were widely spread around the target. The neutron flux determines the neutron transport equation in the moderator and reflector regions. Figures 2a, 2b, 2c, and 2d show the neutron differential flux in terms of energy for neutrons at all energies and separately for fast neutrons in three regions of the neutron activator using a graphite reflector for both lead and bismuth moderators. The total fluxes at all energies were greater in the graphite than in the lead or bismuth and boron regions. The fast and epithermal fluxes increased continuously and gradually because the moderation process in the lead region had a lower slope ratio than that in the graphite region. Figures 3a and 3b show a comparison of the accumulated flux inside two types of moderators using a graphite reflector for neutrons at all energies and for fast neutrons. The accumulated flux using the same reflector indicated that the bismuth moderator can increase the flux a little more than the lead moderator for very fast neutrons. On the contrary, this feature for fast and epithermal neutrons revealed that this property can significantly affect the ^{99}Mo production yield by slow and sure moderation.

Figures 4a, 4b, 4c, and 4d demonstrate the neutron differential flux spectrum in three regions of the neutron activator using the PbF_2 reflector for lead and bismuth moderators in the total and fast ranges. The total fluxes at the whole energy were greater in the PbF_2 region than in the lead or bismuth and boron regions. Figures 5a and 5b show a

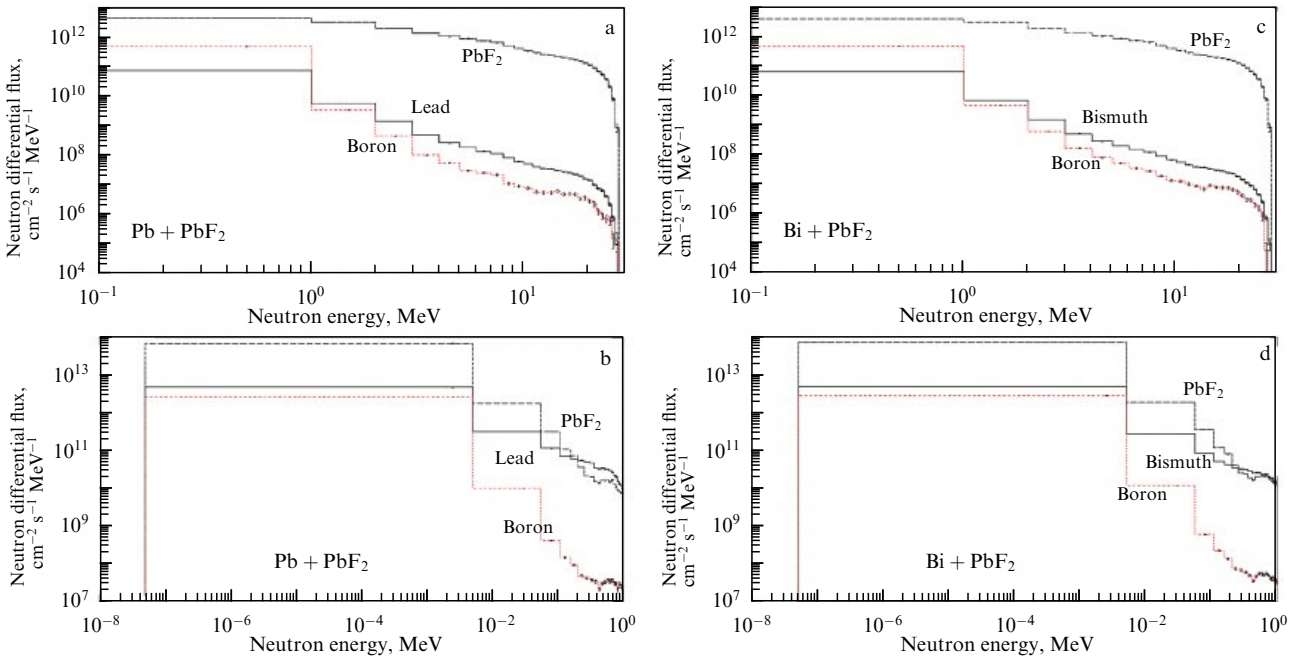

Figure 4. (a) Total flux of neutrons inside lead, PbF_2, and boron regions using PbF_2 reflector. (b) Fast neutron flux inside lead, PbF_2, and boron regions using PbF_2 reflector. (c) Total flux of neutrons inside bismuth, PbF_2, and boron regions using PbF_2 reflector. (d) Fast neutron flux inside bismuth, PbF_2, and boron regions using PbF_2 reflector.

comparison of fluxes inside two types of moderators using the PbF_2 reflector in the total and fast ranges. In the fast and epithermal ranges, bismuth acted slightly more weakly than the lead moderator. This is how this trait can influence the ^{99}Mo production yield.

Comparing Figs 3b and 5b indicates that the accumulated flux in the fast range (5 keV–1 MeV) using lead was somewhat greater than that using bismuth for both reflectors. Also, tuning the neutron energy towards greater saturation yields by more moderation in the epithermal range (0.1 eV–5 keV) shows more emphasis on the neutron flux by applying the bismuth moderator and graphite reflector.

Table 1 presents the simulated outcomes for the neutron flux for four energy ranges (thermal, epithermal, fast, and very fast) and also the total neutron flux within the various regions for different materials and configurations of incident protons at an energy of 30 MeV and current of 300 μA. The epithermal range is significant for ^{99}Mo production, where compact resonance peaks are available. The maximum epithermal flux occurred for the bismuth moderator and the graphite reflector scheme.

3.2 Assessment of the sample thickness and position in activity and production yield

Milli-structure-^{98}Mo samples 1 mm and 2 mm in thickness were inserted into different regions of the simulated activator. The ^{99}Mo production yield and activity depended on the sample position relative to the target at the origin, the moderator/reflector materials, the sample thickness, and the gathered neutron flux. Table 2 shows the activity from the (n, γ) reaction and production yield per sample mass for 1 mm thickness of ^{98}Mo samples in the x, y, and z directions according to Fig. 1. The data in Table 2 were tabulated for two moderators using a graphite reflector for incident protons on the target at an energy of 30 MeV and current of 300 μA. The maximum activity in the moderator region occurred at a distance of 25 cm from the target in the $+x$ direction for the lead moderator and at $z = 15$ cm using the bismuth moderator. A comparison of the two types of moderators indicated that the production yield increased to 2.97×10^4 MBq g^{-1} for the lead moderator, to be compared with a maximum activity of 2.39×10^4 MBq g^{-1} for the bismuth moderator. When the sample was inserted into the graphite region, the maximum activity and yield occurred at $y = -38$ cm and $x = 38$ cm for lead and bismuth moderators, respectively.

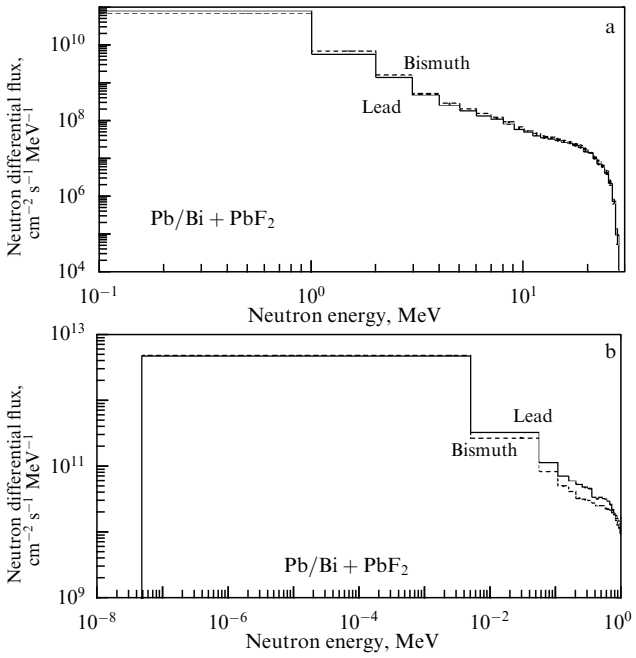

Figure 5. (a) Total flux of neutrons using a PbF_2 reflector for the comparison of lead and bismuth moderators. (b) Neutron flux using a PbF_2 reflector for the comparison of lead and bismuth moderators in the fast range.

Table 2 also shows the activity and yield for ^{98}Mo samples 2 mm in thickness in different positions in the activator using a graphite reflector for two moderators. A comparison of the sample thickness shows that the maximum yield in the moderator region, 3.39×10^4 MBq g^{-1}, occurred at $y = -25$ cm in the direction of the incident proton for the lead and graphite scenarios. When a thicker sample was placed inside the reflector region, the production yield improved for both moderators. The comparison in Table 2 for 1 mm and 2 mm thick samples indicates that the yield was greater with the bismuth moderator when the thicker sample was placed in the graphite reflector.

Table 3 demonstrates the activity and yield using a PbF_2 reflector for two activator schemes with lead and bismuth moderators of ^{98}Mo samples 0.1 cm and 0.2 cm in thickness at various positions. These comparisons indicate that the greatest production yield, 5.03×10^5 MBq g^{-1}, is achieved within

Table 1. Neutron flux (cm^{-2} s^{-1}) in different regions of the activator for four scenarios.

Material/Scenario	Thermal 0–0.1 eV	Epithermal 0.1 eV–5 keV	Fast 5 keV–1 MeV	Very fast 1–30 MeV	Total 0–30 MeV
Pb	1.16×10^{10}	2.93×10^{10}	7.30×10^{10}	8.15×10^{10}	8.15×10^{10}
C	3.36×10^{11}	4.80×10^{11}	5.28×10^{11}	5.31×10^{11}	5.31×10^{11}
B	1.17×10^{10}	1.36×10^{10}	1.36×10^{10}	1.36×10^{10}	1.36×10^{10}
Bi	2.59×10^{10}	4.40×10^{10}	7.70×10^{10}	8.71×10^{10}	8.71×10^{10}
C	4.44×10^{11}	6.00×10^{11}	6.53×10^{11}	6.57×10^{11}	6.57×10^{11}
B	1.45×10^{10}	1.68×10^{10}	1.69×10^{10}	1.69×10^{10}	1.69×10^{10}
Pb	1.56×10^{9}	2.40×10^{10}	7.59×10^{10}	8.45×10^{10}	8.45×10^{10}
PbF_2	4.92×10^{10}	3.47×10^{11}	4.75×10^{11}	4.79×10^{11}	4.79×10^{11}
B	3.55×10^{9}	1.34×10^{10}	1.39×10^{10}	1.40×10^{10}	1.40×10^{10}
Bi	2.75×10^{9}	2.42×10^{10}	6.51×10^{10}	7.53×10^{10}	7.53×10^{10}
PbF_2	5.46×10^{10}	3.54×10^{11}	4.90×10^{11}	4.96×10^{11}	4.96×10^{11}
B	3.70×10^{9}	1.39×10^{10}	1.46×10^{10}	1.46×10^{10}	1.46×10^{10}

Table 2. Activity and production yield for samples 0.1 cm and 0.2 cm in radius at various positions using a graphite reflector for two moderators.

Direction and radial distance from target (cm)	Activity, Bq				Production yield MBq g^{-1}			
	Pb		Bi		Pb		Bi	
	0.1 cm	0.2 cm	0.1 cm	0.2 cm	0.1 cm	0.2 cm	0.1 cm	0.2 cm
$x15$	5.57×10^{8}	2.29×10^{9}	3.47×10^{8}	2.07×10^{9}	1.30×10^{4}	6.71×10^{3}	8.13×10^{3}	6.04×10^{3}
$-x15$	7.27×10^{8}	2.61×10^{9}	5.37×10^{8}	2.56×10^{9}	1.70×10^{4}	7.63×10^{3}	1.26×10^{4}	7.48×10^{3}
$-y15$	7.53×10^{8}	3.62×10^{9}	6.03×10^{8}	2.42×10^{9}	1.76×10^{4}	1.06×10^{4}	1.41×10^{4}	7.09×10^{3}
$z15$	5.45×10^{8}	3.57×10^{9}	1.02×10^{9}	2.56×10^{9}	1.28×10^{4}	1.04×10^{4}	2.39×10^{4}	7.48×10^{3}
$-z15$	3.05×10^{8}	1.60×10^{9}	4.80×10^{8}	1.95×10^{9}	7.13×10^{3}	4.68×10^{3}	1.12×10^{4}	5.70×10^{3}
$x25$	1.27×10^{9}	1.54×10^{9}	4.03×10^{8}	1.55×10^{9}	2.97×10^{4}	4.50×10^{3}	9.45×10^{3}	4.55×10^{3}
$-x25$	6.61×10^{8}	1.95×10^{9}	4.81×10^{8}	1.76×10^{9}	1.55×10^{4}	5.70×10^{3}	1.13×10^{4}	5.16×10^{3}
$-y25$	3.41×10^{8}	1.16×10^{10}	4.47×10^{8}	1.45×10^{9}	7.98×10^{3}	3.39×10^{4}	1.05×10^{4}	4.23×10^{3}
$z25$	2.06×10^{8}	9.14×10^{9}	4.59×10^{8}	1.88×10^{9}	4.83×10^{3}	2.67×10^{4}	1.07×10^{4}	5.51×10^{3}
$-z25$	3.35×10^{8}	1.17×10^{9}	3.53×10^{8}	3.49×10^{9}	7.84×10^{3}	3.44×10^{3}	8.27×10^{3}	1.02×10^{4}
$x38$	1.75×10^{8}	5.65×10^{9}	1.06×10^{9}	2.86×10^{9}	4.10×10^{3}	1.65×10^{4}	2.49×10^{4}	8.36×10^{3}
$-x38$	2.69×10^{8}	1.10×10^{9}	4.02×10^{8}	1.19×10^{9}	6.31×10^{3}	3.21×10^{3}	9.42×10^{3}	3.48×10^{3}
$-y38$	6.98×10^{8}	2.43×10^{9}	2.99×10^{8}	1.57×10^{9}	1.63×10^{4}	7.11×10^{3}	6.99×10^{3}	4.60×10^{3}
$z38$	3.82×10^{8}	1.22×10^{9}	4.76×10^{8}	1.22×10^{9}	8.96×10^{3}	3.57×10^{3}	1.11×10^{4}	3.58×10^{3}
$-z38$	2.51×10^{8}	1.52×10^{9}	2.30×10^{8}	1.24×10^{9}	5.88×10^{3}	4.46×10^{3}	5.38×10^{3}	3.62×10^{3}
$x45$	5.48×10^{7}	8.69×10^{8}	1.68×10^{8}	9.21×10^{8}	1.28×10^{3}	2.54×10^{3}	3.94×10^{3}	2.69×10^{3}
$-x45$	2.43×10^{8}	1.18×10^{10}	3.11×10^{8}	1.30×10^{10}	5.69×10^{3}	3.45×10^{4}	7.27×10^{3}	3.80×10^{4}
$-y45$	1.50×10^{8}	7.25×10^{8}	2.55×10^{8}	1.22×10^{9}	3.52×10^{3}	2.12×10^{3}	5.98×10^{3}	3.57×10^{3}
$z45$	4.06×10^{8}	1.29×10^{9}	2.84×10^{8}	1.03×10^{9}	9.52×10^{3}	3.77×10^{3}	6.66×10^{3}	3.02×10^{3}
$-z45$	9.42×10^{7}	6.63×10^{8}	2.77×10^{8}	1.50×10^{9}	2.21×10^{3}	1.94×10^{3}	6.49×10^{3}	4.37×10^{3}
$x55$	4.08×10^{7}	1.18×10^{9}	7.69×10^{7}	5.06×10^{8}	9.56×10^{2}	3.46×10^{3}	1.80×10^{3}	1.48×10^{3}
$-x55$	1.21×10^{8}	4.55×10^{8}	1.47×10^{8}	6.06×10^{8}	2.83×10^{3}	1.33×10^{3}	3.44×10^{3}	1.77×10^{3}
$-y55$	1.24×10^{8}	9.24×10^{8}	1.22×10^{8}	7.16×10^{8}	2.91×10^{3}	2.70×10^{3}	2.85×10^{3}	2.09×10^{3}
$z55$	2.84×10^{8}	1.37×10^{9}	2.65×10^{7}	3.69×10^{8}	6.65×10^{3}	4.01×10^{3}	6.21×10^{2}	1.08×10^{3}
$-z55$	2.09×10^{8}	3.95×10^{8}	8.01×10^{7}	6.42×10^{8}	4.90×10^{3}	1.15×10^{3}	1.88×10^{3}	1.88×10^{3}

Table 3. Activity and production yield for samples 0.1 cm and 0.2 cm in radius at various positions using a PbF_2 reflector for two moderators.

Direction and radial distance from target (cm)	Activity, Bq				Production yield, MBq g^{-1}			
	Pb		Bi		Pb		Bi	
	0.1 cm	0.2 cm	0.1 cm	0.2 cm	0.1 cm	0.2 cm	0.1 cm	0.2 cm
$x15$	3.09×10^{8}	7.13×10^{3}	1.60×10^{8}	1.47×10^{9}	7.25×10^{3}	7.13×10^{3}	3.76×10^{3}	4.29×10^{3}
$-x15$	4.52×10^{8}	2.93×10^{9}	3.97×10^{8}	1.25×10^{9}	1.06×10^{4}	8.57×10^{3}	9.31×10^{3}	3.66×10^{3}
$-y15$	2.64×10^{9}	5.36×10^{9}	5.26×10^{8}	2.55×10^{9}	6.19×10^{4}	1.57×10^{4}	1.23×10^{4}	7.47×10^{3}
$z15$	5.77×10^{8}	3.38×10^{9}	4.68×10^{8}	9.95×10^{9}	1.35×10^{4}	9.87×10^{3}	1.10×10^{4}	2.91×10^{4}
$-z15$	3.05×10^{8}	2.02×10^{9}	2.30×10^{8}	4.78×10^{9}	7.14×10^{3}	5.91×10^{3}	5.39×10^{3}	1.40×10^{4}
$x25$	3.46×10^{8}	1.10×10^{9}	2.76×10^{8}	1.45×10^{9}	8.10×10^{3}	3.22×10^{3}	6.46×10^{3}	4.23×10^{3}
$-x25$	2.31×10^{8}	1.10×10^{9}	4.52×10^{8}	2.49×10^{9}	5.41×10^{3}	3.21×10^{3}	1.06×10^{4}	7.29×10^{3}
$-y25$	5.19×10^{9}	1.30×10^{10}	4.87×10^{8}	1.38×10^{9}	1.22×10^{5}	3.79×10^{4}	1.14×10^{4}	4.03×10^{3}
$z25$	1.94×10^{8}	1.58×10^{9}	1.43×10^{9}	2.16×10^{9}	4.53×10^{3}	4.62×10^{3}	3.34×10^{4}	6.33×10^{3}
$-z25$	3.01×10^{8}	7.76×10^{8}	5.19×10^{9}	4.62×10^{9}	7.04×10^{3}	2.27×10^{3}	1.22×10^{5}	1.35×10^{4}
$x38$	2.09×10^{10}	4.48×10^{10}	1.40×10^{9}	2.09×10^{9}	4.90×10^{5}	1.31×10^{5}	3.27×10^{4}	6.12×10^{3}
$-x38$	7.18×10^{8}	3.90×10^{9}	5.79×10^{8}	1.05×10^{9}	1.68×10^{4}	1.14×10^{4}	1.36×10^{4}	3.06×10^{3}
$-y38$	1.41×10^{8}	7.86×10^{8}	1.24×10^{8}	7.71×10^{8}	3.30×10^{3}	2.30×10^{3}	2.90×10^{3}	2.25×10^{3}
$z38$	7.94×10^{7}	3.63×10^{8}	3.09×10^{8}	6.46×10^{8}	1.86×10^{3}	1.06×10^{3}	7.24×10^{3}	1.89×10^{3}
$-z38$	1.43×10^{9}	5.98×10^{9}	2.15×10^{10}	4.74×10^{10}	3.34×10^{4}	1.75×10^{4}	5.03×10^{5}	1.39×10^{5}
$x45$	4.02×10^{8}	1.67×10^{9}	9.97×10^{7}	1.23×10^{9}	9.43×10^{3}	4.89×10^{3}	2.34×10^{3}	3.58×10^{3}
$-x45$	8.63×10^{7}	2.68×10^{8}	7.36×10^{7}	4.99×10^{8}	2.02×10^{3}	7.84×10^{2}	1.72×10^{3}	1.46×10^{3}
$-y45$	6.03×10^{7}	3.83×10^{8}	1.45×10^{7}	6.69×10^{8}	1.41×10^{3}	1.12×10^{3}	3.41×10^{2}	1.96×10^{3}
$z45$	1.29×10^{8}	5.79×10^{8}	6.07×10^{6}	1.81×10^{10}	3.03×10^{3}	1.69×10^{3}	1.42×10^{2}	5.29×10^{4}
$-z45$	4.17×10^{7}	1.78×10^{9}	5.88×10^{7}	4.32×10^{8}	9.75×10^{2}	5.21×10^{3}	1.38×10^{3}	1.26×10^{3}
$x55$	1.03×10^{7}	1.45×10^{9}	2.83×10^{7}	2.36×10^{9}	2.41×10^{2}	4.25×10^{3}	6.62×10^{2}	6.91×10^{3}
$-x55$	6.54×10^{7}	9.11×10^{8}	8.88×10^{5}	6.35×10^{7}	1.53×10^{3}	2.66×10^{3}	2.08×10^{1}	1.86×10^{2}
$-y55$	4.58×10^{7}	2.57×10^{8}	1.58×10^{7}	1.29×10^{8}	1.07×10^{3}	7.50×10^{2}	3.71×10^{2}	3.76×10^{2}
$z55$	4.48×10^{6}	2.31×10^{9}	8.82×10^{6}	1.24×10^{8}	1.05×10^{2}	6.75×10^{3}	2.07×10^{2}	3.62×10^{2}
$-z55$	5.68×10^{7}	1.33×10^{8}	1.01×10^{7}	1.53×10^{8}	1.33×10^{3}	3.88×10^{2}	2.37×10^{2}	4.48×10^{2}

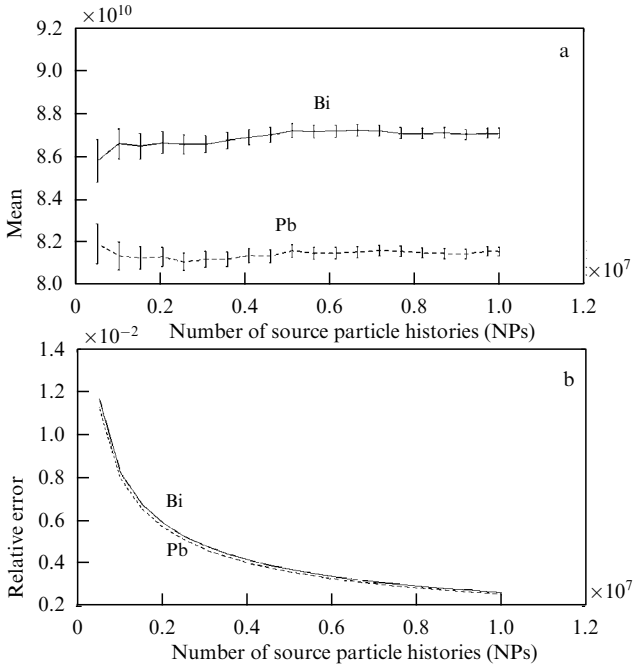

Figure 6. (a) The variation of tally mean with 10^7 histories for bismuth and lead moderators. (b) The relative error of F4 tally with 10^7 histories for bismuth and lead moderators.

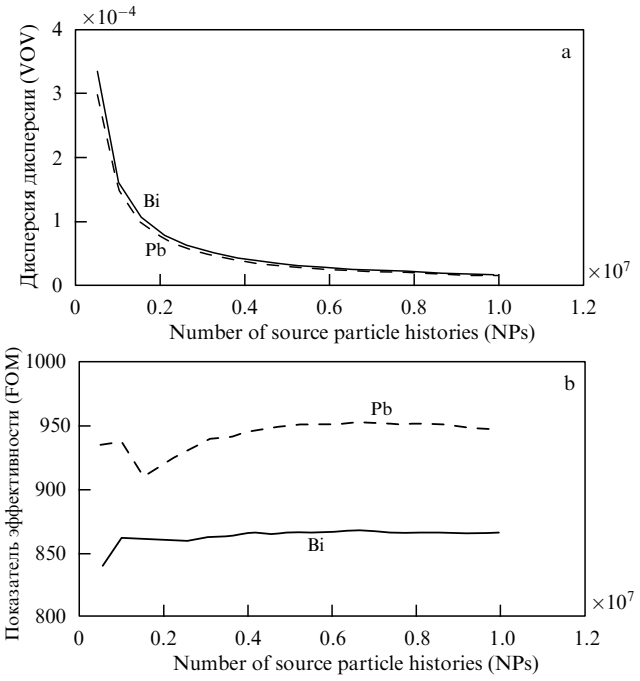

Figure 7. (a) VOV performance as $1/N$ for bismuth and lead moderators. (b) FOM variations are relatively constant for 10^7 histories for bismuth and lead moderators.

the reflector region (PbF_2) using the bismuth moderator and 0.1 cm sample thickness at $z = -38$ cm.

The results reveal that when the ^{98}Mo sample was placed inside the reflector region, the radiative capture yield increased because of a greater gathered epithermal neutron flux. Furthermore, these simulations confirmed that the production yield is greater for a bismuth moderator and PbF_2 reflector in comparison with other proposed schemes.

3.3 Statistical parameters of the MCNP output

The additional outputs of MCNP assist in evaluating a series of tests carried out. The tally mean $\bar{x}$ exhibited random fluctuations in terms of the number of source particle histories (NPS) around approximately 8.6×10^{10}, as shown in Fig. 6a for a bismuth moderator. This parameter was approximately 8.2×10^{10} for the lead moderator. The mean tally indicated no considerable up or down trends. The relative error parameter ought to be less than 0.1 for the quality of the tally evaluation. According to Fig. 6b, as the NPS increases, R decreases monotonically as $1/\sqrt{N}$ for bismuth and lead materials.

The magnitude of the VOV must be less than 0.1 for the tally, and this parameter is displayed in Fig. 7a as a function of the number of particle histories. The VOV parameter decreases monotonically as $1/N$, while the NPS increases for both moderators. The FOM values remain nearly constant for the output data. Figure 7b shows the FOM as a function of NPS for both moderators, for which this parameter exhibited no monotonic upward or downward trends.

The statistical parameters describe the dependability of the records. Sometimes, the tally is underestimated without any sampling of a number of high-scoring rare events in the history run. If a rare event with a large score is sampled, the R and FOM parameters significantly increase and decrease, respectively.

3.4 Discussion

Accelerators have been used as an alternative in radioisotope production, particularly for ^{99}Mo. The routine method is based on a standard nuclear reactor, but the proposed method is based on neutron energy tuning until production locally occurs by an activator. The simulated result proved that the energy and flux of moderated neutrons can satisfy some radioisotope production trials. In this method, the ^{99}Mo production process was based on the appropriate flux in the epithermal range and distinctive physical characteristics of materials in the activator. Therefore, using the proposed schemes and sample location inside the suggested moderator or reflector regions could be significant for achieving a high and proper yield.

The high atomic mass of the proposed moderators, lead and bismuth, has led to an increase in the neutron energy loss in elastic scattering. These materials are distinguished by their high level of transparency to fast neutrons, for which a long time is required before they reach the proper energy. The moderator region is bulky enough to reduce neutron leakage from the activator. In addition, the designed reflector saves the neutrons. This allows the use of molybdenum-resonance peaks to capture attuned neutrons.

Importantly, the ARC method was examined via the slowing down of induced neutrons from a very high energy to the suitable and final epithermal energy during collisions with the nuclei of lead/bismuth moderators and graphite/PbF_2 reflectors. These neutron collisions and energy losses were recorded as a successive process, which is suitable if the reduced energy ratio is small for molybdenum transmutation. The logarithmic energy decrement is defined as the energy ratio of the original source after a collision. This parameter is known as lethargy. The mean lethargy of neutrons is small because of the high atomic mass of the used moderators, bismuth and lead, in addition to a large elastic cross section,

which is independent of the energy. Therefore, different or hybrid moderators could be used because neutron transport in diverse materials occurs with different diffusion coefficients. Prospective research warrants the investigation of the impurities in the moderator material for the assessment of transmutation using some other radioisotopes like rhenium and gold [40, 41].

Remarkably, transmutation was investigated here via an inserted ^{98}Mo 'father radioisotope' with millimeter thickness inside the activator at various radial distances from the target. The physical shape of the sample or the sample thickness and geometry should be such that self-absorption is minimal. Therefore, diminishing the flux and neutron capture inside the sample due to the self-absorption effect could be examined via thinner/thicker samples to optimize the system. The activity and saturation yield for the (n, xn) reaction are much smaller than for the (n, γ) reaction by virtue of diverse neutron cross section behaviors at very fast and thermal ranges in transmutation. The fast neutron spectrum affects the molybdenum transmutation procedure with a low chance of other Mo isotopes being contaminated because of the simulated high purity of ^{98}Mo and also incompatible fast neutron spectra in the capture process. Technologies to obtain high-purity ^{98}Mo from natural molybdenum with different geochemical characteristics [42] may cost the system choice. In this study, as an indirect production technique in the accelerator-based method, the effect of other molybdenum isotopes being contaminated is remarkably low compared to the direct or reactor-based methods.

The direct method in the $^{100}\mathrm{Mo}(p, 2n)^{99m}\mathrm{Tc}$ reaction, where an incident proton beam hits an ^{100}Mo sample directly and technetium is produced straightforwardly, would result in concomitant production of minor Tc radio-impurities depending on the isotopic composition of the sample material, the proton beam energy, and the irradiation time [43–48]. It was demonstrated in [43] and [44] that the saturation yield per μA of incident proton by 16.5 MeV is 2.7×10^3 MBq and remains constant between 2 and 6 hours of irradiation. Because the cross section for this direct reaction reaches approximately 1 barn at the 18 MeV proton energy and the proton range in molybdenum at 18 MeV is 0.065 cm, the yield based on extrapolation of the estimated data is anticipated to be 3.8×10^3 MBq μA^{-1} [47]. This yield per microampere would definitely exceed that for an energy of 30 MeV.

On the other hand, the indirect method using the $^{100}\mathrm{Mo}(n, 2n)^{99}\mathrm{Mo}$ reaction usually involves energetic protons or deuterons bombarding a carbon target. In this reaction, the neutron cross section is 1.5 barn at the 16 MeV neutron energy and is 66 times less than the neutron cross section of ^{98}Mo in the epithermal range for radiative capture. Although this cross section is 10 times larger than the thermal neutron capture cross section of ^{98}Mo, it was demonstrated in [49] by irradiating an enriched ^{100}Mo sample for 198 h with a neutron flux of 1×10^{13} n cm^{-2} s^{-1} at the 14 MeV neutron energy after 1 h cooling that one can produce the specific activity of ^{99}Mo as high as 7.9×10^4 MBq g^{-1}. Because only 9.6% of natural Mo is ^{100}Mo and there are seven other stable Mo isotopes, the ^{100}Mo enrichment process is expensive to use the maximum $(n, 2n)$ reaction cross section of 1.5 barn [50, 51]. Here, a comparison revealed that the difference in production yield at saturation is between 10^4 and 10^5 MBq g^{-1}.

In the reactor-based method, fission Mo has the potential to be contaminated with fission products, uranium and transuranium elements. Therefore, the specification of radionuclidic impurity is more stringent and complicated than for the (n, γ) reaction. Although energetic neutrons can affect the yield in an accelerator-based method, the (n, γ) reaction just includes 'suitable' neutrons with maximum probability, greater than 100 barn, in the resonance range 10^{-2}–10^{-4} MeV. Simulation results revealed that the ^{99}Mo production yield is greater for a bismuth moderator and PbF_2 reflector than for other proposed schemes.

4. Conclusions

Tuning of moderated neutrons for radioisotope production is based on the activator design and the materials used. We suggested using low-energy/current protons from a small cyclotron to achieve a suitable saturation yield of molybdenum. Moreover, using graphite/PbF_2 reflectors could help in the energy tuning of neutrons. The neutron moderator material was also investigated. As regards the potential for the production of more sophisticated radioisotopes, or the possibility of competing with reactor-produced ones, this way is more accessible and safer. If the moderation and reflection processes are correctly controlled, a neutron activator can be used for boron neutron capture therapy applications under collimation surveillance. Therefore, an empirical procedure can be suggested because of the benefits of using small cyclotrons rather than the standard nuclear reactor for neutron collimation and then producing beta emitter radioisotopes in hospitals.

Acknowledgments

I thank the people of Gerash for their spiritual and financial support in founding Gerash University of Medical Sciences, the Amir-al-Momenin Hospital, the Cancer Prevention Center, the MRI department, specialized and relevant laboratories, and well-equipped residences in the Fars province of Iran. I also thank all the benefactors on this occasion, especially Haj Molla-Hossein Khorshidi and Halimeh Khajehpour. And finally, I appreciate all the charity organizations in Gerash that give social and financial support for the poor across Iran and work with low levels of government aid in public health and welfare.

References

1. Bobeica M et al. *Romanian Rep. Phys.* **68** S847 (2016)
2. Radioisotopes in Medicine, World Nuclear Association (June 2018), https://www.world-nuclear.org/information-library/non-power-nuclear-applications/radioisotopes-research/radioisotopes-in-medicine.aspx
3. "Feasibility of producing molybdenum-99 on a small scale using fission of low enriched uranium or neutron activation of natural molybdenum", Technical Reports Series No. 478 (Vienna: Intern. Atomic Energy Agency, 2015)
4. Zhuikov B L *Phys. Usp.* **59** 481 (2016); *Usp. Fiz. Nauk* **186** 544 (2016)
5. Khorshidi A et al. *J. Nucl. Med. Technol.* **40** 37 (2012)
6. Khorshidi A et al. *Prog. Biophys. Mol. Biol.* **109** 59 (2012)
7. Khorshidi A, Ashoor M *Ann. Nucl. Med.* **28** 363 (2014)
8. Ashoor M et al. *Indian J. Nucl. Med.* **30** 239 (2015)
9. Nabipour J S, Khorshidi A *J. Med. Imaging Radiat. Oncol.* **49** 194 (2018)
10. Ashoor M, Khorshidi A *Proc. Natl. Acad. Sci. India Sect. A Phys. Sci.* (2018) https://doi.org/10.1007/s40010-018-0482-x
11. Khorshidi A, Ahmadinejad M, Hosseini S H *Medicine* **94** e1098 (2015)

12. Khorshidi A *Cancer Biotherapy Radiopharm.* **30** 317 (2015)
13. Khorshidi A *J. Cancer Res. Therapy.* **13** 456 (2017)
14. Ashoor M, Khorshidi A *Am. J. Roentgenol.* **206** 455 (2016)
15. ''The supply of medical radioisotopes. 2017 medical isotope supply review: ^{99}Mo/^{99m}Tc market demand and production capacity projection 2017-2022'', Nuclear Development NEA/SEN/HLGMR 2017-2 (Paris: OECD Nuclear Energy Agency, 2017); https://www.oecd-nea.org/med-radio/docs/sen-hlgmr2017-2.pdf
16. Stavissky Yu Ya *Phys. Usp.* **49** 1253 (2006); *Usp. Fiz. Nauk* **176** 1283 (2006)
17. Rubbia C ''Resonance enhanced neutron captures for element activation and waste transmutation'', CERN-LHC-97-004-EET (Geneva: CERN, 1997); https://cds.cern.ch/record/329843
18. Arnould H et al. (TARC Collab.) ''Neutron driven nuclear transmutation by adiabatic resonance crossing'', CERN-SL-99-036-EET (Geneva: CERN, 1999); http://cds.cern.ch/record/403959
19. Abánades A et al. *Nucl. Instrum. Meth. Phys. Res. A* **478** 577 (2002)
20. Khorshidi A *Instrum. Exp. Tech.* **61** (2) 198 (2018)
21. Yurov D V, Prikhodko V V *Phys. Usp.* **57** 1118 (2014); *Usp. Fiz. Nauk* **184** 1237 (2014)
22. Rubbia C et al. ''Conceptual design of a fast neutron operated high power energy amplifier'', CERN-AT-95-44-ET (Geneva: CERN, 1995)
23. Revol J-P *Phys. Usp.* **46** 725 (2003); *Usp. Fiz. Nauk* **173** 747 (2003)
24. Kadi Y, Herrera-Martinez A *Nucl. Instrum. Meth. Phys. Res. A* **562** 573 (2006)
25. Kadi Y *Prog. Nucl. Energy* **49** 606 (2007)
26. Khorshidi A et al. *J. Radioanal. Nucl. Chem.* **299** 303 (2014)
27. Khorshidi A *Mater. Sci. Eng. C* **68** 449 (2016)
28. Froment P et al. *Nucl. Instrum. Meth. Phys. Res. A* **493** 165 (2002)
29. Abbas K et al. *Nucl. Instrum. Meth. Phys. Res. A* **601** 223 (2009)
30. Brett D, Owen H, Gill M ''Resonant neutron capture for radioisotope production'', Interim Report (Manchester: Univ. of Manchester, 2010)
31. ''MCNPX^{TM} user's manual version 2.6.0'', Technical Report LA-CP-07-1473 (Ed. D B Pelowitz) (Los Alamos, NM: Los Alamos National Laboratory, 2008)
32. ANSYS, Inc. Manual documents to Ansys 12.0 (Canonsburg, PA: ANSYS Inc., 2009)
33. Strelkov A V *Phys. Usp.* **47** 511 (2004); *Usp. Fiz. Nauk* **174** 565 (2004)
34. Tolstov K D ''Some Aspects of Accelerator Breeding'', JINR preprint, 18-89-778 (Dubna: OIYaI, 1989)
35. Stacey W M *Nuclear Reactor Physics* 2nd ed. (Weinheim: Wiley-VCH, 2007)
36. Apse V et al. *Lead Containing Mainly Isotope 208PB New Neutron Moderator, Coolant and Reflector for Innovative Nuclear Reactors* (Moscow: NRNU, 2011)
37. Lamarsh J R, Baratta A J *Introduction to Nuclear Engineering* 3rd ed. (Upper Saddle River, NJ: Prentice Hall, 2001)
38. Aksenov V L *Phys. Usp.* **52** 406 (2009); *Usp. Fiz. Nauk* **179** 434 (2009)
39. Shultis J K, Faw R E *An MCNP Primer* (Manhattan, KS: Kansas State Univ., 2011)
40. Plekhanov V G *Phys. Usp.* **43** 1147 (2000); *Usp. Fiz. Nauk* **170** 1245 (2000)
41. Akulinichev S V *Phys. Usp.* **57** 1239 (2014); *Usp. Fiz. Nauk* **184** 1363 (2014)
42. Khorshidi A, Soltani Nabipour J *Braz. J. Rad. Sci.* **5** (2) 1 (2017)
43. Celler A et al. *Phys. Med. Biol.* **56** 5469 (2011)
44. Gagnon K et al. *Nucl. Med. Biol.* **38** 907 (2011)
45. Lebeda O, Pruszyński M *Appl. Radiat. Isotop.* **68** 2355 (2010)
46. Guérin B et al. *J. Nucl. Med.* **51** 13N (2010)
47. Bénard F et al. *J. Nucl. Med.* **55** 1017 (2014)
48. Khorshidi A et al. *Phys. Scr.* **89** 095001 (2014)
49. Nagai Y, Hatsukawa Y *J. Phys. Soc. Jpn.* **78** 033201 (2009)
50. Gopalakrishna A et al. *J. Radioanal. Nucl. Chem.* **316** 561 (2018)
51. Takács S et al. *Nucl. Instrum Meth. Phys. Res. B* **347** 26 (2015)